




## Article

# Crystal Structure of Novel Terephthalate Salt of Antiarrhythmic Drug Disopyramide

Majid Ismail Tamboli <sup>†</sup>, Yohei Utusmi <sup>†</sup>, Takayuki Furuishi <sup>\*†</sup> , Kaori Fukuzawa  and Etsuo Yonemochi <sup>\*†</sup> 

Department of Physical Chemistry, School of Pharmacy and Pharmaceutical Sciences, Hoshi University, 2-4-41 Ebara, Shinagawa-ku, Tokyo 142-8501, Japan; t-majid@hoshi.ac.jp (M.I.T.); s172504@hoshi.ac.jp (Y.U.); k-fukuzawa@hoshi.ac.jp (K.F.)

\* Correspondence: t-furuishi@hoshi.ac.jp (T.F.); e-yonemochi@hoshi.ac.jp (E.Y.); Tel.: +81-3-5498-5159 (T.F.); +81-3-5498-5048 (E.Y.)

<sup>†</sup> Co-first author, these authors contributed equally to this work.

**Abstract:** 1:1 salt of Disopyramide (DPA) with Terephthalic acid (TA) was obtained by the slow solvent evaporation and the slurry crystallization methods. X-ray single crystal diffraction of DPA:TA confirmed the formation of salt by the transfer of an acidic proton from one of the carboxylic acid groups of TA to the tertiary amino group of the chain moiety (N3-nitrogen atom) of the DPA molecules. DPA:TA salt crystals crystallize in the triclinic system with space group *P*-1. The asymmetric unit, comprising one protonated DPA and one TA anion, are linked by a strong charge assisted N<sup>+</sup>–H···O<sup>−</sup> hydrogen bond and a C–H···O<sup>−</sup> hydrogen bond. Moreover, structural characterization of DPA:TA salt was carried out using Fourier transform infrared spectroscopy, differential scanning calorimeter, thermogravimetric analysis, and powder X-ray diffraction techniques

**Keywords:** Disopyramide; Terephthalic acid; salt; crystal structure; molecular packing; slurry crystallization



**Citation:** Tamboli, M.I.; Utusmi, Y.; Furuishi, T.; Fukuzawa, K.; Yonemochi, E. Crystal Structure of Novel Terephthalate Salt of Antiarrhythmic Drug Disopyramide. *Crystals* **2021**, *11*, 368. <https://doi.org/10.3390/cryst11040368>

Academic Editor: Sławomir J. Grabowski

Received: 28 February 2021  
Accepted: 28 March 2021  
Published: 31 March 2021

**Publisher's Note:** MDPI stays neutral with regard to jurisdictional claims in published maps and institutional affiliations.



**Copyright:** © 2021 by the authors. Licensee MDPI, Basel, Switzerland. This article is an open access article distributed under the terms and conditions of the Creative Commons Attribution (CC BY) license (<https://creativecommons.org/licenses/by/4.0/>).

## 1. Introduction

Crystal engineering deals with the study of non-covalent interactions within crystals, the understanding of crystal structures, and the design and synthesis of new solids with desired and specific properties by utilizing the hydrogen bond, supramolecular synthon strategy [1–5]. Crystal engineering approaches have been used in the preparation of novel solid active forms of pharmaceutical ingredients (APIs), for improving the physicochemical properties of drug molecules by making multi-component crystals, such as solvates [6], cocrystals [7–9], and salts [10]. In the supramolecular synthon strategy in the pharmaceutical field, salt formation of APIs remains a potential method to improve the solubility and stability of native APIs.

Disopyramide (2-diisopropylaminoethyl)-phenyl-2-pyridineacetamide (DPA) is a class IA antiarrhythmic drug [11] that shows polymorphism behavior [12]. Disopyramide and its phosphate salt are intravenously and orally administered for clinical use [13,14]. There is very limited research on the crystal engineering of DPA available in the literature [15], and there are only limited DPA phosphate salt [16] crystal structures of solid forms of DPA to be found in the Cambridge Structural Database (CSD). DPA has a basic nature and is likely to form salts/cocrystal adduct with different cofomers that have acid functionality. Moreover, DPA has a flexible molecular framework, with a hydrogen bond donor and acceptor site, and can adopt different orientations or conformations in the novel solid form; hence, from a crystal engineering viewpoint, DPA could be a molecules that has the potential for the exploration of different solid forms by the use of crystal engineering principles.

With this in mind, our intention is to explore the novel solid form of DPA by using different acidic cofomers and to see their effect on the conformation of DPA and molecular

packing in crystal structures, because there is only one crystal structure of DPA phosphate salt reported by Kawamura and Hirayama [16] in the CSD. In the current study, we have selected Terephthalic acid (TA) as the salt former, which has a para disubstituted carboxyl group on the benzene ring (Figure 1). In this article, we discuss the preparation method of DPA:TA salt and carry out X-ray single-crystal structural analysis; the obtained new salt was further evaluated by solid-state characterization.

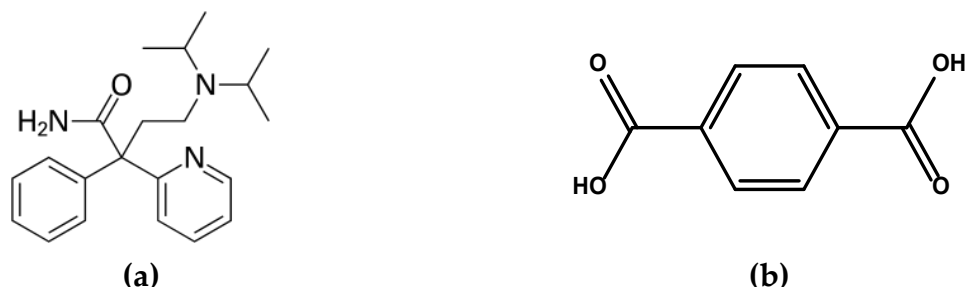


**Figure 1.** Structures of (a) racemic Disopyramide (DPA) and (b) Terephthalic acid (TA).

## 2. Materials and Methods

### 2.1. Materials

DPA and TA were purchased from Tokyo Chemical Industry Co. Ltd. (Tokyo, Japan). All other analytical-grade solvents and reagents were commercially obtained and used without further purification.

### 2.2. Crystallization of DPA:TA Salt

#### 2.2.1. Slow Evaporation Method

For X-ray single-crystal structure analysis, DPA (0.5 mmole) and TA (0.5 mmole) in a 1:1 molar ratio were ground in a mortar and pestle for 10 min to obtain a fine powder, then a few drops of ethanol were added to it, before grinding again for 10–15 min to obtain a powder. From this, 50 mg was used for the crystallization experiment. Colorless single crystals suitable for single crystal X-ray diffraction were obtained by dissolving the 50 mg of ground material in 15 mL acetonitrile and 5 mL ethanol under sonication at a temperature of 50 °C for 1 h. The resulting solution, obtained after filtration, was left for slow evaporation at ambient conditions for 4–6 weeks to obtain a long plate-like crystal, which was stuck on the wall of the flask.

#### 2.2.2. Slurry Method

Reproducing the salt crystal was found to be difficult, so another method for crystallization was used. Luckily, similar solid salt is easily obtained by the slurry method. One mmole each of DPA and TA were weighed at a molar ratio of 1:1 and suspended in 50 mL acetonitrile in a 250 mL conical flask. The resulting suspension was stirred in a magnetic stirrer at 25 °C, 500 rpm for about 36 h until a white solid material precipitated out. The resulting suspension was filtered to isolate the white solid, which was then air dried for 5–6 days at ambient conditions before being used for further analysis. Powder X-ray diffraction (PXRD) patterns of the isolated solids matched the simulated PXRD pattern obtained from single crystal data DPA:TA, suggesting that both were the same solid form.

### 2.3. Single-Crystal X-ray Diffraction

The single-crystal X-ray diffraction data for DPA:TA salt was collected at 93 K. The measurements were carried out in  $\omega$ -scan mode with an R-AXIS RAPID II (Rigaku Co., Tokyo, Japan) with the Cu-K $\alpha$  X-ray obtained from rotating the anode source with a graphite monochromator. The integrated and scaled data were empirically corrected for absorption effects using ABSCOR [17,18]. The structures were solved by direct methods using SHELXS and refinement was carried out by full-matrix least-squares technique using SHELXL [19,20]. All non-hydrogen atoms were refined anisotropically. The hydrogen atom

attached to the nitrogen N2, N3, and O4 atoms in the DPA:TA salt were located using the differential Fourier map and refined isotropically. All other hydrogen atom positions were calculated geometrically and included in the calculation using the riding atom model.

The molecular figures were produced and prepared using Mercury 4.1.0 software [21]. CCDC 2065287 contains the supplementary crystallographic data for the DPA:TA salt and can be obtained free of charge from the Cambridge Crystallographic Data Centre via [www.ccdc.cam.ac.uk/data\\_request/cif](http://www.ccdc.cam.ac.uk/data_request/cif) (accessed on 28 March 2021).

#### 2.4. PXRD

The PXRD patterns of the DPA:TA samples were measured in the reflectance mode using a SmartLab diffractometer (Cu K $\alpha$  source (40 kV and 200 mA), D/teX ultra-high-speed position-sensitive detector, Rigaku, Tokyo, Japan). Diffraction patterns (2 $\theta$ ) were collected from 5° to 40° at 25°C with a step of 0.01° and a scan speed of 20°/min.

#### 2.5. Fourier Transform Infrared Spectroscopy (FT-IR)

The infrared spectra of all samples were measured using FT-IR (FT-IR- 4200 spectrometer, JASCO Co., Tokyo, Japan) with an attenuated total reflection (ATR) unit (ATR-PRO 670H-S, JASCO Co., Tokyo, Japan). The recorded spectrum represents an average of 64 scans obtained with a resolution of 4 cm<sup>-1</sup> at room temperature. The spectra were collected in wavenumbers ranging from 4000 to 400 cm<sup>-1</sup>. The internal reflectance element used in this study was a diamond trapezoid having 45° entrance and exit faces.

#### 2.6. Differential Scanning Calorimetry (DSC) and Thermogravimetric (TG) Measurements

DSC and TG measurements were recorded with a Thermo plus EVO2-DSC 8230 and a Thermo plus EVO2-TG8120 TG-DTA, respectively (Rigaku Co., Tokyo, Japan). The DSC sample (~3 mg) was placed into an aluminum-crimped pan and the TG sample (~4–5 mg) was placed into an aluminum-open pan, and both were measured at a speed of 5°C/min from 25 to 300°C under nitrogen gas (flow rate = 50 and 100 L/min, respectively).

### 3. Results and Discussion

#### 3.1. Crystal Structure of DPA:TA Salt

TA and DPA in a 1:1 molar ratio were crystallized from acetonitrile and ethanol mixtures at ambient condition by slow solvent evaporation to obtain a colorless long plate crystal suitable for X-ray analysis. The X-ray single-crystal structure confirmed the formation of DPA:TA salt with approximately similar C–O bond lengths of C28–O2, 1.2538 (19), C28–O3, 1.268 (2), Å of the (COO<sup>-</sup>) carboxylate group of TA (Figure 2a). These similarities in the bond length of C–O confirmed the transfer of an acidic proton from one of the carboxylic acidic group of TA to the N3-nitrogen atom of the tertiary amino group (chain moiety) of DPA.

DPA:TA salt crystallized in the centrosymmetric triclinic *P*-1 space group containing one protonated DPA and one TA anion in the asymmetric unit revealed that the molecular salt is in the 1:1 molar ratio. The salt pair, i.e., the protonated DPA and TA anion in the asymmetric unit linked by a strong charge, assisted the N3<sup>+</sup>–H3A···O2<sup>-</sup> hydrogen bond and the C9–H9···O3<sup>-</sup> hydrogen bond. In the crystal structure of DPA:TA salt, protonated DPA displays an intramolecular N2–H2A···N1 hydrogen bond by donating second amide hydrogen N–H to the N-atom of 2-pyridine moiety in the S<sup>1</sup><sub>1</sub>(6) ring motif, along with other C–H···O intramolecular interactions, namely C15–H15B···O1 and C17–H17B···O1, which stabilize the conformation protonated DPA molecules in the salt, as shown in Figure 2a. The crystallographic information and geometrical parameters for the hydrogen bonding interaction are summarized in Tables 1 and 2.

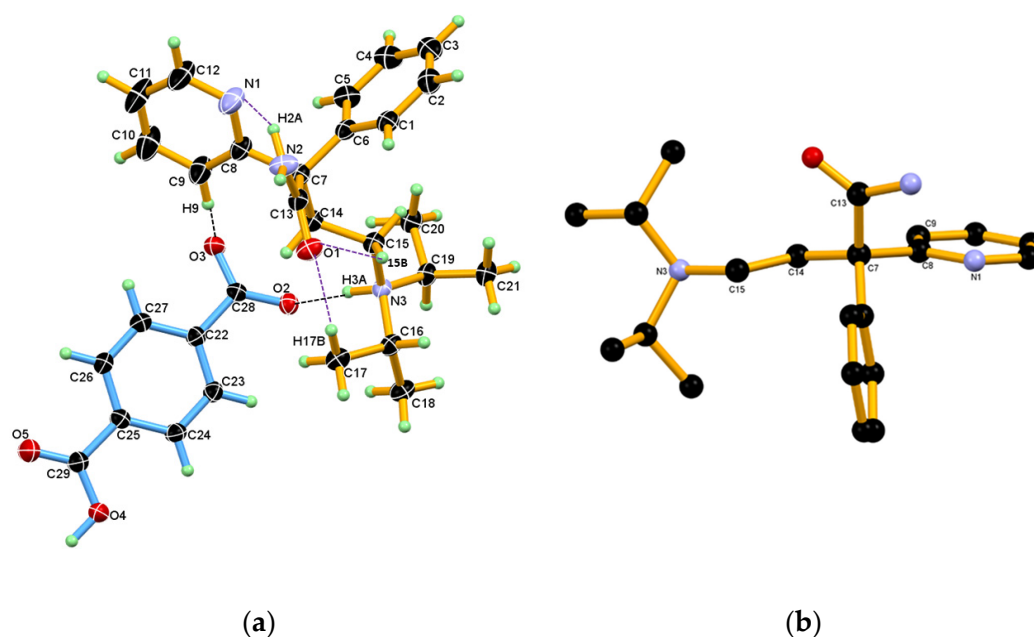


**Figure 2.** (a) ORTEP diagram of DPA:TA salt showing the atom numbering scheme. The thermal ellipsoid is drawn at 50% probability level, and H-atoms are shown as small spheres with arbitrary radii. The association between the salt pair in the asymmetric unit of DPA:TA salt is shown by the black dotted line and, in this association, only the carboxylate group of TA is involved. Protonated DPA in salt displaying the intramolecular N2-H2A...N1, C15-H15B...O1, C17-H17B...O1 hydrogen bond is shown by the purple dotted line. (b) Conformation of protonated DPA in salt and torsional angle  $\tau_1$ —C7—C14—C15—N3,  $\tau_2$ —C8—C7—C14—C15,  $\tau_3$ —C9—C8—C7—C14,  $\tau_4$ —C13—C7—C14—C15.

**Table 1.** Crystallographic data table for the DPA:TA salt.

Parameters	DPA:TA
Empirical formula	C <sub>29</sub> H <sub>35</sub> N <sub>3</sub> O <sub>5</sub>
Formula weight	505.60
Temperature	93(2) K
Wavelength	1.54187 Å
Crystal system	Triclinic
Space group	<i>P</i> -1
Unit cell dimensions	$a = 8.6855(2)$ Å, $\alpha = 100.640(7)^\circ$ $b = 9.7036(3)$ Å, $\beta = 103.230(7)^\circ$ $c = 17.1705(4)$ Å, $\gamma = 91.205(6)^\circ$
Volume	1381.48(8) Å <sup>3</sup>
<i>Z</i> , <i>Z'</i>	2.1
Density (calculated)	1.215 g/cm <sup>3</sup>
Absorption coefficient	0.676 mm <sup>-1</sup>
<i>F</i> (000)	540.0
Crystal size	0.460 × 0.420 × 0.220 mm <sup>3</sup>
Theta range for data collection	4.647 to 68.224°
Index ranges	−10 ≤ <i>h</i> ≤ 10, −11 ≤ <i>k</i> ≤ 11, −20 ≤ <i>l</i> ≤ 20
Reflections collected	16230
Independent reflections	4955 [ <i>R</i> <sub>int</sub> = 0.0307, <i>R</i> <sub>sigma</sub> = 0.0411]
Completeness to theta = 67.687°	98.1 %
Absorption correction	Semi-empirical from equivalents
Max. and min. transmission	0.862 and 0.67
Refinement method	Full-matrix least-squares on <i>F</i> <sup>2</sup>
Data/restraints/parameters	4955/0/354
Goodness-of-fit on <i>F</i> <sup>2</sup>	1.078
Final <i>R</i> indices [ <i>I</i> > 2σ( <i>I</i> )]	<i>R</i> <sub>1</sub> = 0.0478, <i>wR</i> <sub>2</sub> = 0.1280
<i>R</i> indices (all data)	<i>R</i> <sub>1</sub> = 0.0555, <i>wR</i> <sub>2</sub> = 0.1337
Δρ <sub>max</sub> , Δρ <sub>min</sub>	0.32/−0.25 e. Å <sup>-3</sup>



**Table 2.** Geometrical parameters of the hydrogen bond interaction in DPA:TA salt.

D-H...A	D-H (Å)	H...A (Å)	D...A (Å)	D-H...A (°)	Symmetry Codes
N2-H2A...N1	0.934(19)	2.076(18)	2.783(3)	131.4(16)	Intramolecular
N2-H2B...O1	0.88(2)	2.00(2)	2.876(2)	176(2)	2 - x, 1 - y, 1 - z
N3-H3A...O2	0.946(18)	1.821(18)	2.7617(18)	172.5(17)	x, y, z
O4-H4A...O3	0.96(3)	1.57(3)	2.5211(18)	176(2)	x, -1 + y, z
C9-H9...O3	0.95	2.58	3.389(2)	143	x, y, z
C15-H15B...O1	0.99	2.41	3.008(2)	118	Intramolecular
C16-H16...O3	1.00	2.50	3.499(2)	176	1 + x, y, z
C17-H17B...O1	0.98	2.49	3.469(2)	173	Intramolecular
C20-H20B...O4	0.98	2.48	3.344(2)	147	x, 1 + y, z
C21-H21C...O5	0.98	2.57	3.478(2)	154	1 + x, 1 + y, z
C19-H19...O2	1.00	2.609	3.2976(18)	126.02	1 - x, 1 - y, -z
C20-H20C...O2	0.98	2.693	3.3375(19)	123.65	1 - x, 1 - y, -z

In the DPA:TA salt, DPA adopts conformation, where the 2-pyridine ring moiety is roughly coplanar with the chain moiety (excluding the iso-propyl moiety), and the phenyl moiety is oriented roughly perpendicular to the planar part, as shown in Figure 2b. In the DPA:TA salt, the torsional angle  $\tau_1$  179.38,  $\tau_2$  170.70 suggests planarity in the backbone chain, and torsional angle  $\tau_3$  (12.75) suggests slight twist in the coplanarity between the chain moiety and the 2-pyridine moiety.

The dihedral angle between the phenyl and pyridine rings is 78.76(10) in DPA:TA salt, suggesting a nearly perpendicular orientation. However, the torsional value  $\tau_4$  (-71.52) is for the orientation of the amide group, with the planar part also being roughly perpendicular.

In the crystal structure of DPA:TA salt, two inversion-symmetry related protonated DPA molecules form an amide homodimer synthon via a pair of strong N-H...O hydrogen bonds in the  $R^2_2(8)$  ring motif, and they are listed in Table 2. In this dimeric association, protonated DPA donates amide hydrogen N2-H2B to the amide C=O1 oxygen of inversion-symmetry related protonated DPA molecules in the dimeric N2-H2B...O1 hydrogen bond, whereas the second hydrogen of amide N2-H2A engaged in the intramolecular N2-H2A...N1 nitrogen bonds with the N1-atom of the 2-pyridine moiety in the  $S^1_1(6)$  ring motif. This homodimer of protonated DPA molecules were linked to two TA anion via a strong charge assisted N3<sup>+</sup>-H3A...O2<sup>-</sup> hydrogen bond and the C9-H9...O3<sup>-</sup> interaction to form a centrosymmetric dimeric unit comprising two protonated DPA and two TA anion, as shown in Figure 3a. In this association, N<sup>+</sup>3-H3A (protonated tertiary amino nitrogen) hydrogen of the protonated DPA donates hydrogen to carboxylate (COO<sup>-</sup>) O2-oxygen of the TA anion in the N3<sup>+</sup>-H3A...O2<sup>-</sup> hydrogen bond, and the C9-H9 Hydrogen of the 2-pyridine moiety donates hydrogen to carboxylate (COO<sup>-</sup>) O3-oxygen of the TA anion in the C9-H9...O3 interaction. Thus, in this association, both carboxylate (COO<sup>-</sup>) O2-, O3-oxygen of TA anion are engaged in hydrogen bonding with protonated DPA molecules, as shown in Figure 3a. The closely associated TA anion forms a one-dimensional (1D) chain using a linear and strong O4-H4A...O3<sup>-</sup> hydrogen bond, as shown in Figure 3b.

Such dimeric units are extended through linear and strong O4-H4A...O3<sup>-</sup> and short and non-linear C20-H20B...O4 hydrogen bonds with the neighboring unit translated dimeric units along the *b*-axis to generate a ladder-like network where the protonated DPA dimer units join the 1D chains of the TA anion, as shown in Figure 4. In this association, the O3<sup>-</sup> oxygen atom of the carboxylate anion of TA accepts hydrogen from the carboxyl OH (O4-H4A) of the neighboring unit translated TA anion in the O4-H4A...O3<sup>-</sup> hydrogen bond along the *b*-axis. Whereas, in turn, carboxyl hydroxyl (O4-H4A) O4-oxygen accept C20-H20B hydrogen of unit translated protonated DPA molecules in short and non-linear C20-H20B...O4 hydrogen bonds.

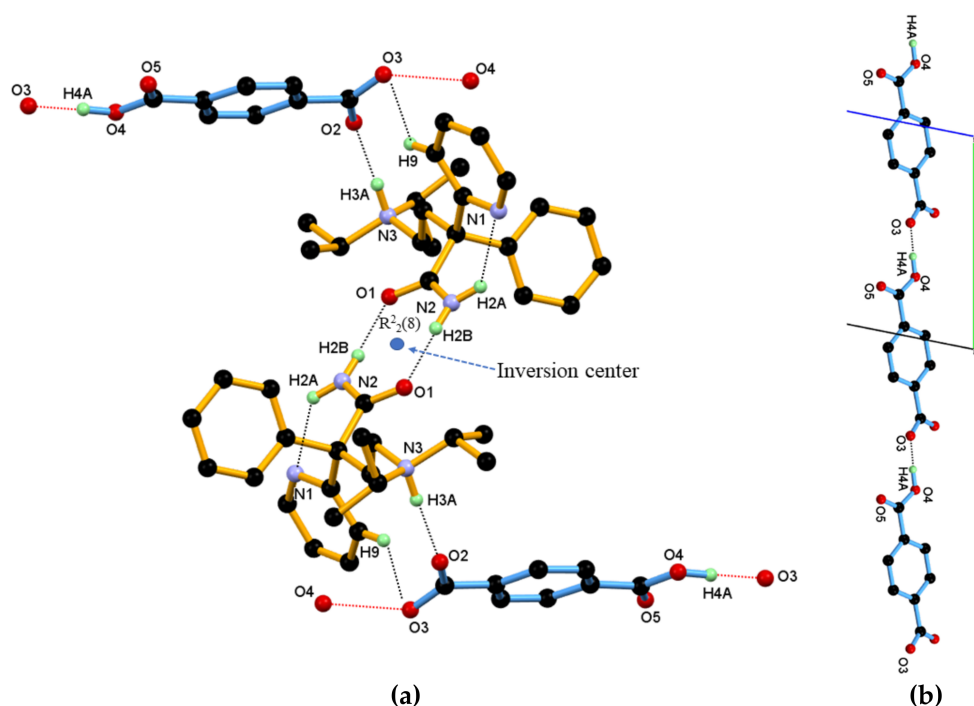


**Figure 3.** (a) Dimeric unit of DPA:TA salt. In this, the inversion center related asymmetric unit of DPA:TA extends through the N–H $\cdots$ O hydrogen bond in the  $R^2_2(8)$  ring motif in  $ac$ -diagonally. (b) TA anion linked to neighboring unit translated TA anion through a strong and linear O4–H4A $\cdots$ O3 $^-$  hydrogen bond to form a one-dimensional (1D) chain of TA anion along the  $b$ -axis. Dotted lines indicate the non-covalent interaction (hydrogen atoms not involved in the hydrogen bonding were removed for clarity).

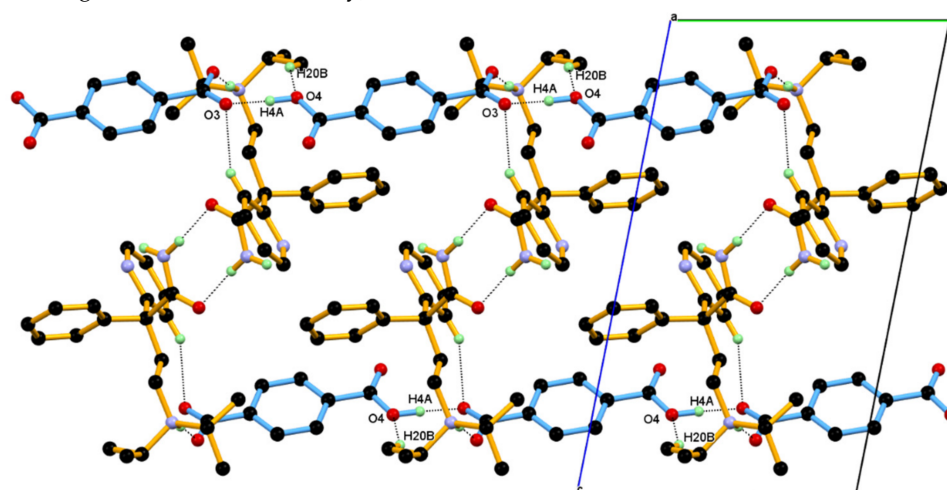


**Figure 4.** Linking of neighboring unit translated dimeric units along the  $b$ -axis through O4–H4 $\cdots$ O3 $^-$  and C20–H20B $\cdots$ O4 hydrogen bonding interaction to form a ladder structure along the  $b$ -axis. In this packing, the protonated DPA dimer is held between the 1D chain of the TA anion.

Such 1D chains of dimeric units (ladder-like structures), assembled along the  $a$ -axis to generate two-dimensional (2D) layer packing through C16–H16 $\cdots$ O3 $^-$ , C21–H21C $\cdots$ O5 interaction, generate a 2D layer. In this association, the *iso*-propyl moiety of protonated DPA molecules are involved in C–H $\cdots$ O hydrogen bonding by donating C16–H16 and C21–H21 hydrogen to the carboxylate oxygen O3 and carboxyl (C=O5) oxygen of the neighboring 1D chain of dimeric units along the  $a$ -axis, as shown in Figure 5a. Whereas the packing of such 1D chains of dimeric units (ladder-like structures) along the  $ac$ -diagonal are done through relatively weak and longer C–H $\cdots$ O interaction by donating C19–H19

and C20–H20 hydrogen of the *iso*-propyl moiety of protonated DPA molecules to the carboxylate oxygen O2 of the TA anion from the neighboring 1D chain of dimeric units through C19–H19...O2<sup>−</sup> and C20–H20C...O2<sup>−</sup> interaction, as shown in Figure 5b.

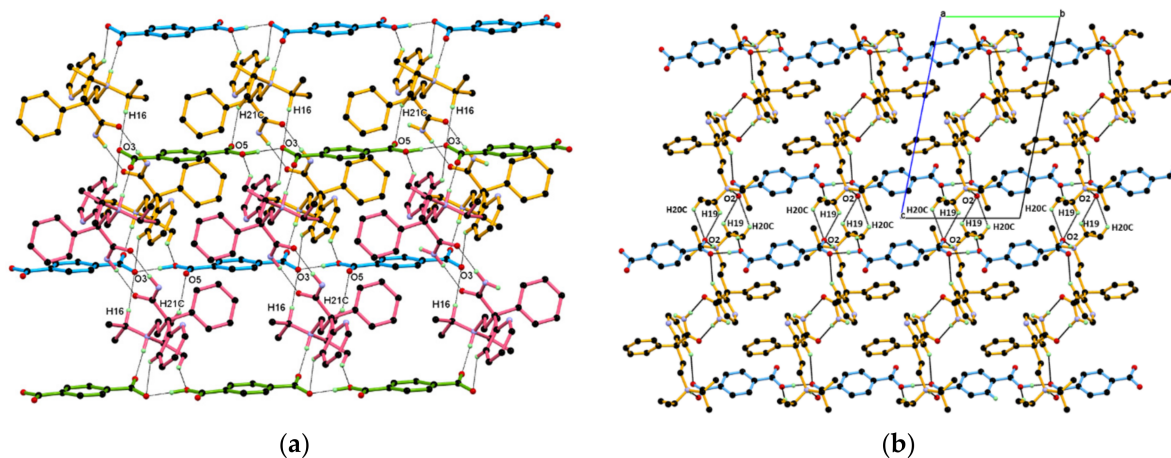


**Figure 5.** Packing of the 1D dimeric unit chain (a) along the *a*-axis through C16–H16...O3<sup>−</sup>, C21–H21C...O5 interaction to generate a two-dimensional (2D) layer (b) along the *ac*-diagonal through C19–H19...O2<sup>−</sup> and C20–H20C...O2<sup>−</sup> interaction to generate a 2D layer.

Packing the view down the *b*-axis, in this packing, the dimeric unit is associated with the neighboring dimeric unit along the *a*-axis (parallel to the *ac*-diagonal) through short C16–H16...O3<sup>−</sup> interaction; in this association, the *iso*-propyl moiety of the protonated DPA donates C16–H16 hydrogen to the carboxylate O3-oxygen of the TA anion of the neighboring dimeric unit. Whereas, along the *ac*-diagonal dimeric unit, the DPA:TA associated centrosymmetric combine with the neighboring dimeric unit through relatively weaker and longer C–H...O interactions by donating C19–H19 and C20–H20C hydrogen of the *iso*-propyl moiety of the protonated DPA molecules to the carboxylate O2-oxygen of the TA anion from the neighboring dimeric unit through C19–H19...O2<sup>−</sup> and C20–H20C...O2<sup>−</sup> interactions, as shown in Figure 6. Packing of the 1D chain of dimeric units in the *ac*-plane creates a solvent assessable void and void space ~22 Å<sup>3</sup> per molecule (asymmetric unit) in the unit cell, calculated by using the contact surface from Mercury 2020, 2.0 software.

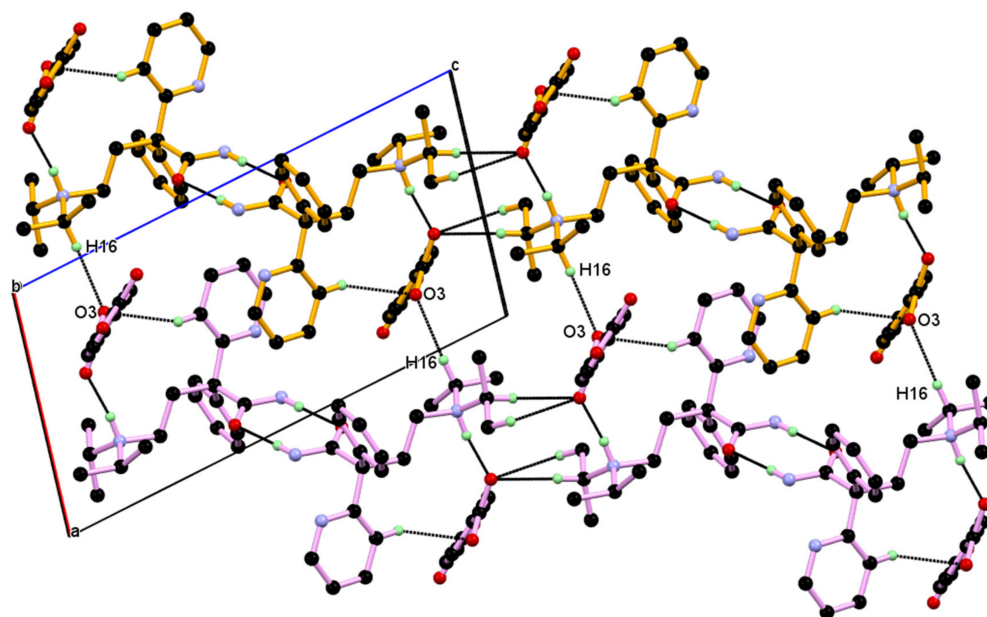


**Figure 6.** Packing of dimeric unit view down the *b*-axis. The neighboring dimeric unit is associated through C–H...O interaction.

### 3.2. Characterization of DPA:TA Salt

#### 3.2.1. PXRD

The PXRD patterns were recorded for commercially available DPA, TA, and DPA:TA crystals obtained from slow solvent evaporation and DPA:TA salt obtained from the slurry method. The PXRD pattern of the salt is different from the DPA component, suggesting the formation of a new crystalline phase in the solid-state. (Figure 7). Furthermore, the peak position of the experimental PXRD pattern obtained from the slow solvent evaporation and the slurry method matched well with the simulated PXRD pattern obtained from the single-crystal X-ray structure, confirming the homogeneity of the sample and ruling out the presence of another phase. It also confirms that the single-crystal structure is representative of the bulk and that there is no phase transition between 93 K (at which the single-crystal structure was determined) and room temperature (at which the powder pattern was measured). The subtle differences could be due to the different data collection temperatures (for powder and a single crystal). Thus, a PXRD analysis of samples obtained by the slurring of DPA and TA in acetonitrile at 25 °C is matched very well to the DPA:TA salt obtained from the slow evaporation methods, which indicated a similar solid form of salt DPA:TA obtained from both methods.

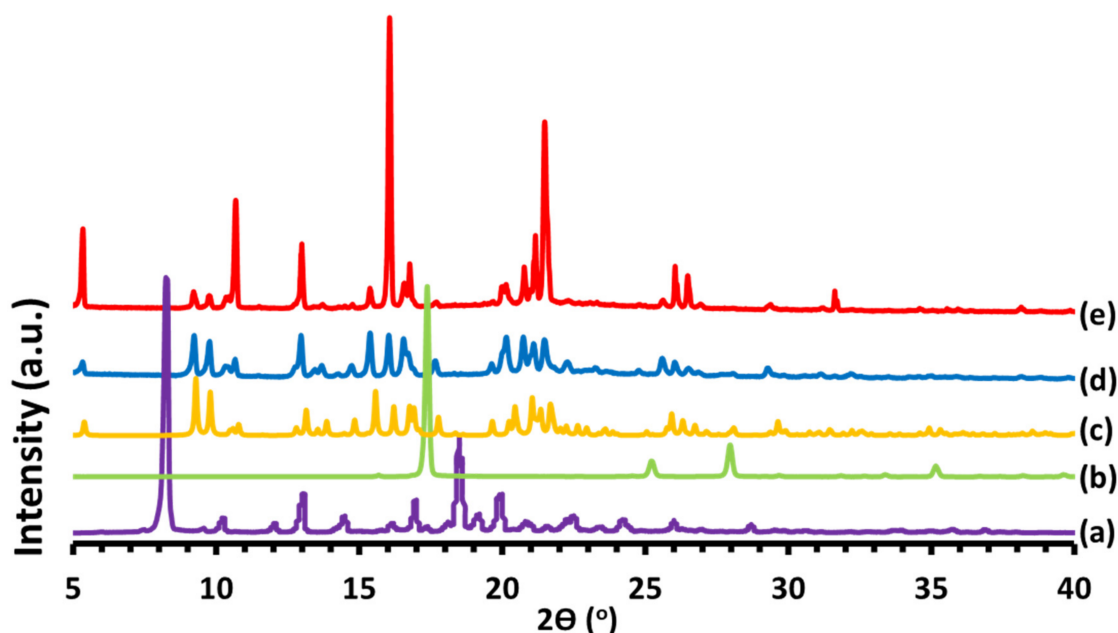


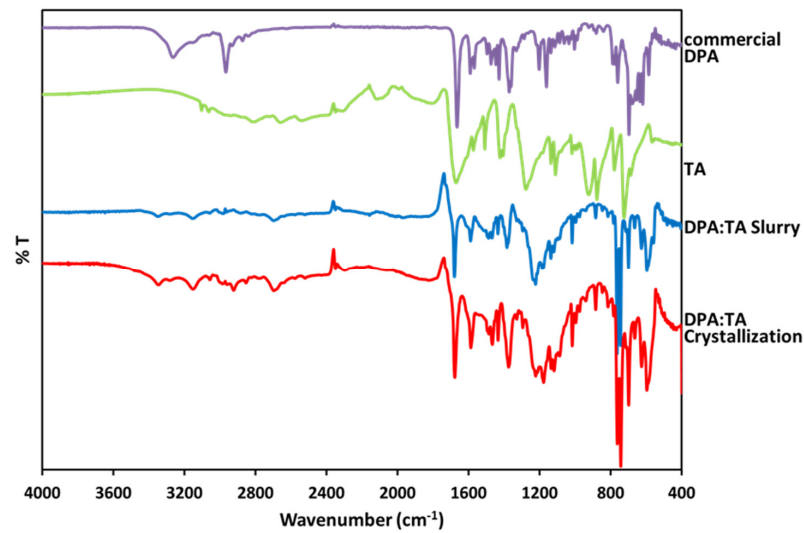
**Figure 7.** Powder X-ray diffraction (PXRD) patterns of (a) commercial DPA, (b) TA, (c) simulated DPA:TA, (d) DPA:TA salt obtained from slurry method, and (e) DPA:TA salt obtained from slow solvent evaporation.

#### 3.2.2. FT-IR Spectrum

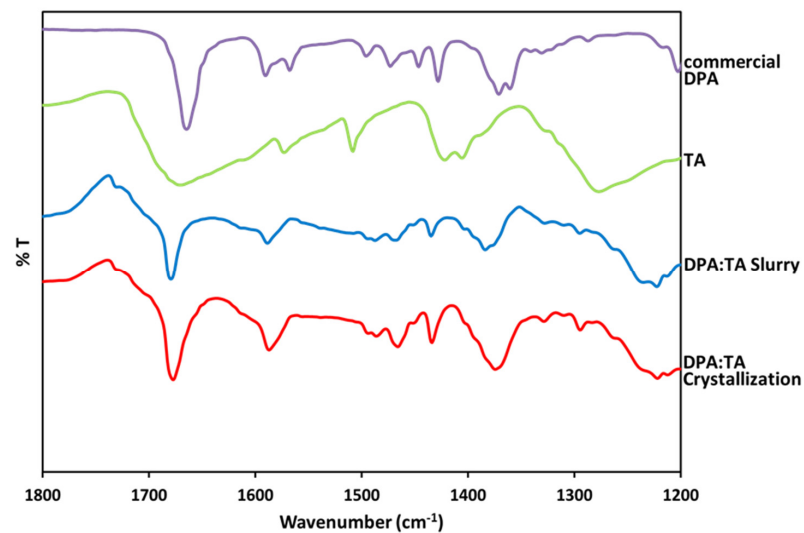
FT-IR is a very important and useful techniques for detecting the formation of salt by the typical carboxylate anion present in spectra (Figure 8). Due to changes in the hydrogen bonding patterns of a molecule in salt or a co-crystal, there are resulting changes in the IR frequencies of vibrations associated with the functional groups. The changes in IR frequencies suggest changes in hydrogen bonding pattern. Examination of FT-IR spectra could confirm salt formation due to the transfer of acidic hydrogen TA to DPA.

FT-IR spectra were obtained for commercially pure DPA, prepared DPA:TA crystal, pure TA, and DPA:TA salt obtained from the slurry method. Commercially pure DPA demonstrated characteristic peaks, amide N-H stretching at  $3263\text{ cm}^{-1}$ , amide C=O stretching, and  $\text{NH}_2$  deformation overlap peak at  $1664\text{ cm}^{-1}$ , and in TA spectra presently peak at  $1671\text{ cm}^{-1}$  due to C=O stretching and broad band around  $2800\text{ cm}^{-1}$ , attributed to the carboxylic OH group [22]. Whereas the spectra of salt give many characteristic peaks as 3350, 3149,

1679, and 1589  $\text{cm}^{-1}$  that are different from the starting component DPA and TA shown in Figure 8.



(a)



(b)

**Figure 8.** FT-IR spectra, (a) 4000–400  $\text{cm}^{-1}$  and (b) 1800–1200  $\text{cm}^{-1}$ , of commercial DPA, TA, and DPA:TA salt obtained from the slurry method and DPA:TA salt obtained from the slow evaporation method.

Thus, in DPA:TA salt, the spectrum peaks at 1589  $\text{cm}^{-1}$ ; where the carboxylate group is observed respectively and is not present in the spectrum of the individual components, which indicates a proton transfer from the salt former TA to DPA, confirming salt formation between DPA and TA.

### 3.2.3. Thermal Properties

The thermal behavior of the DPA:TA was measured by DSC and TG. DPA:TA salt, exhibits a sharp, single endothermic peak at around 181  $^{\circ}\text{C}$ , corresponding to melting point of salt in DSC (Figure 9). It has been reported that there are two melting points of DPA; a low-melting type crystal (85–87  $^{\circ}\text{C}$ ) and a high-melting type crystal (95–98  $^{\circ}\text{C}$ ) [12],



and TA melted with sublimation at around 350 °C [23–25]. DPA:TA showed a different melting point from each starting materials, suggesting that DPA:TA is a novel salt. TG data of DPA:TA revealed that there was no weight loss before melting, which confirmed the absence of any solvent or hydrate in the crystal lattice, as per the single crystal data.

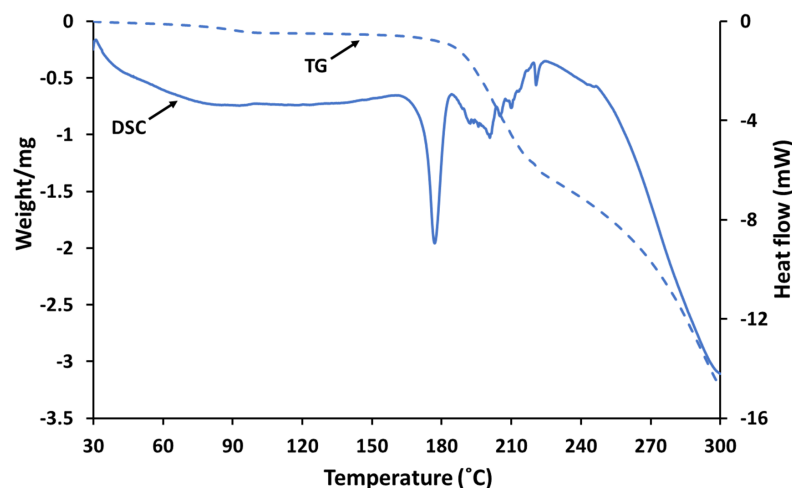


Figure 9. DSC and TG profiles of DPA:TA salt obtained from the slow evaporation method.

#### 4. Conclusions

1:1 DPA:TA salt crystals were obtained from the slow evaporation method, and its crystal structure belongs to the triclinic  $P-1$  space group. The asymmetric unit of 1:1 DPA:TA salt contains one protonated DPA and one TA anion.

In the crystal structure of DPA:TA salt, two inversion symmetry related protonated DPA molecules formed an amide homodimer through a  $N-H\cdots O$  hydrogen bond in the  $R^2_2(8)$  ring motifs, and such a dimer is hydrogen bonded to two TA anions through charge assisted  $N^+-H\cdots O^-$  and  $C-H\cdots O^-$  hydrogen bonds to form a basic centrosymmetric dimeric unit, comprising two protonated DPA and two TA anions. Furthermore, such a dimeric unit linked to a unit translated neighboring dimeric unit along the  $b$ -axis through an  $O3^-\cdots H4-O4$  hydrogen bond between carboxylate  $O3$ -oxygen and the carboxyl ( $O-H$ ) of the next TA anion along the  $b$ -axis results in a one-dimensional chain, which is further supported by  $C20-H20B\cdots O4$  interaction between DPA and TA. Such a 1D chain assembled along the  $a$ -axis through  $C16-H16\cdots O3^-$  and  $C21-H21C\cdots O5$  interaction generates a two-dimensional structure. Such a 2D layer structure, assembled centrosymmetrically along the  $c$ -axis through relatively weaker  $C-H\cdots O$  interactions, results in a 3D layer in the  $ac$ -plane.

**Author Contributions:** Conceptualization, M.I.T.; formal analysis, M.I.T. and Y.U.; investigation, M.I.T. and Y.U.; writing—original draft preparation, M.I.T. and T.F.; writing—review and editing, T.F. and E.Y.; visualization, M.I.T., Y.U., and T.F.; funding acquisition, T.F.; supervision, K.F. and E.Y.; project administration, T.F., K.F., and E.Y. All authors have read and agreed to the published version of the manuscript.

**Funding:** This study was supported by the Mochida Memorial Foundation for Medical and Pharmaceutical Research 2019–2020 (to T.F.).

**Conflicts of Interest:** The authors declare no conflict of interest.

#### References

- Desiraju, G.R. Supramolecular Synthons in Crystal Engineering—A New Organic Synthesis. *Angew. Chem. Int. Ed. Engl.* **1995**, *34*, 2311–2327. [[CrossRef](#)]
- Berry, D.J.; Steed, J.W. Pharmaceutical cocrystals, salts and multicomponent systems; intermolecular interactions and property based design. *Adv. Drug Deliv. Rev.* **2017**, *117*, 3–24. [[CrossRef](#)]

3. Martins, I.C.B.; Sardo, M.; Santos, S.M.; Fernandes, A.; Antunes, A.; André, V.; Mafra, L.; Duarte, M.T. Packing Interactions and Physicochemical Properties of Novel Multicomponent Crystal Forms of the Anti-Inflammatory Azelaic Acid Studied by X-ray and Solid-State NMR. *Cryst. Growth Des.* **2015**, *16*, 154–166. [[CrossRef](#)]
4. Corpinot, M.K.; Bučar, D.-K. A Practical Guide to the Design of Molecular Crystals. *Cryst. Growth Des.* **2018**, *19*, 1426–1453. [[CrossRef](#)]
5. Desiraju, G.R. *Crystal Engineering: The Design of Organic Solids*; Elsevier: Amsterdam, The Netherlands; New York, NY, USA, 1989.
6. Bezerra, B.P.; Pogoda, D.; Perry, M.L.; Vidal, L.M.T.; Zaworotko, M.J.; Ayala, A.P. Cocrystal Polymorphs and Solvates of the Anti-Trypanosoma cruzi Drug Benznidazole with Improved Dissolution Performance. *Cryst. Growth Des.* **2020**, *20*, 4707–4718. [[CrossRef](#)]
7. Karimi-Jafari, M.; Padrela, L.; Walker, G.M.; Croker, D.M. Creating Cocrystals: A Review of Pharmaceutical Cocrystal Preparation Routes and Applications. *Cryst. Growth Des.* **2018**, *18*, 6370–6387. [[CrossRef](#)]
8. Schultheiss, N.; Newman, A. Pharmaceutical Cocrystals and Their Physicochemical Properties. *Cryst. Growth Des.* **2009**, *9*, 2950–2967. [[CrossRef](#)]
9. Yousef, M.A.E.; Vangala, V.R. Pharmaceutical Cocrystals: Molecules, Crystals, Formulations, Medicines. *Cryst. Growth Des.* **2019**, *19*, 7420–7438. [[CrossRef](#)]
10. Gunnam, A.; Nangia, A.K. High-Solubility Salts of the Multiple Sclerosis Drug Teriflunomide. *Cryst. Growth Des.* **2019**, *19*, 5407–5417. [[CrossRef](#)]
11. Katz, M.J.; Meyer, C.E.; El-Etr, A.; Slodki, S.J. Clinical evaluation of a new anti-arrhythmic agent, SC-7031. *Curr. Ther. Res. Clin. Exp.* **1963**, *5*, 343–350. [[PubMed](#)]
12. Gunning, S.R.; Freeman, M.; Stead, J.A. Polymorphism of disopyramide. *J. Pharm. Pharm.* **1976**, *28*, 758–761. [[CrossRef](#)]
13. Rizos, I.; Brachmann, J.; Lengfelder, W.; Schmitt, C.; von Olshausen, K.; Kubler, W.; Senges, J. Effects of intravenous disopyramide and quinidine on normal myocardium and on the characteristics of arrhythmias: Intraindividual comparison in patients with sustained ventricular tachycardia. *Eur. Heart J.* **1987**, *8*, 154–163. [[CrossRef](#)]
14. Kim, S.Y.; Benowitz, N.L. Poisoning due to class IA antiarrhythmic drugs. Quinidine, procainamide and disopyramide. *Drug Saf.* **1990**, *5*, 393–420. [[CrossRef](#)] [[PubMed](#)]
15. Burke, T.R., Jr.; Nelson, W.L.; Mangion, M.; Hite, G.J.; Mokler, C.M.; Ruenitz, P.C. Resolution, absolute configuration, and antiarrhythmic properties of the enantiomers of disopyramide, 4-(diisopropylamino)-2-(2-pyridyl)-2-phenylbutyramide. *J. Med. Chem.* **1980**, *23*, 1044–1048. [[CrossRef](#)]
16. Kawamura, T.; Hirayama, N. Crystal structure of  $\alpha$ -diisopropylaminoethyl- $\alpha$ -phenylpyridine-2- acetamide phosphate, [C<sub>21</sub>H<sub>30</sub>N<sub>3</sub>O][H<sub>2</sub>PO<sub>4</sub>]. *Z. Krist. New Cryst. Struct.* **2011**, *226*, 479. [[CrossRef](#)]
17. Higashi, T. *Calculated Using ABSCOR: Empirical Absorption Correction Based on Fourier Series Approximation*; Rigaku: The Woodland, TX, USA, 1994.
18. Messerschmidt, A.; Schneider, M.; Huber, R. ABSCOR: A scaling and absorption correction program for the FAST area detector diffractometer. *J. Appl. Crystallogr.* **1990**, *23*, 436–439. [[CrossRef](#)]
19. Sheldrick, G.M. SHELXT—Integrated space-group and crystal-structure determination. *Acta Cryst. A Found. Adv.* **2015**, *71*, 3–8. [[CrossRef](#)]
20. Sheldrick, G.M. Crystal structure refinement with SHELXL. *Acta Cryst. C Struct. Chem* **2015**, *71*, 3–8. [[CrossRef](#)]
21. Macrae, C.F.; Bruno, I.J.; Chisholm, J.A.; Edgington, P.R.; McCabe, P.; Pidcock, E.; Rodriguez-Monge, L.; Taylor, R.; van de Streek, J.; Wood, P.A. Mercury CSD 2.0—new features for the visualization and investigation of crystal structures. *J. Appl. Crystallogr.* **2008**, *41*, 466–470. [[CrossRef](#)]
22. Pavia, D.L.; Lampman, G.M.; Kriz, G.S.; Vyvyan, J.A. *Introduction to Spectroscopy*; Cengage Learning: Boston, MA, USA, 2014.
23. Elmas Kimyonok, A.B.; Ulutürk, M. Determination of the Thermal Decomposition Products of Terephthalic Acid by Using Curie-Point Pyrolyzer. *J. Energetic Mater.* **2015**, *34*, 113–122. [[CrossRef](#)]
24. Machado Cruz, R.; Boleslavskaya, T.; Beranek, J.; Tieger, E.; Twamley, B.; Santos-Martinez, M.J.; Dammer, O.; Tajber, L. Identification and Pharmaceutical Characterization of a New Itraconazole Terephthalic Acid Cocrystal. *Pharmaceutics* **2020**, *12*, 741. [[CrossRef](#)] [[PubMed](#)]
25. Ma, Y.-H.; Ge, S.-W.; Wang, W.; Sun, B.-W. Studies on the synthesis, structural characterization, Hirshfeld analysis and stability of apovincamine (API) and its co-crystal (terephthalic acid: Apovincamine=1:2). *J. Mol. Struct.* **2015**, *1097*, 87–97. [[CrossRef](#)]